This is a repository copy of *Identification of a spatio-temporal model of crystal growth based on boundary curvature*.

White Rose Research Online URL for this paper:
http://eprints.whiterose.ac.uk/74622/

eprints@whiterose.ac.uk
https://eprints.whiterose.ac.uk/

Identification of a Spatio-Temporal Model of Crystal Growth Based on Boundary Curvature

Y. Zhao, S. A. Billings, D.Coca, R.Ristic, L.Matos

Disce Doce

RERVM COGNOSCERE CAVSAS

Identification of a Spatio-Temporal Model of Crystal Growth based on Boundary Curvature

Y.Zhao, S.A.Billings, D.Coca *, R.Ristic, L.Matos†

November 15, 2007

Abstract

A new method of identifying the spatio-temporal transition rule of crystal growth is introduced based on the connection between growth kinetics and dentritic morphology. Using a modified three-point-method, curvatures of the considered crystal branch are calculated and curvature direction is used to measure growth velocity. A polynomial model is then produced based on a curvature-velocity relationship to represent the spatio-temporal growth process. A very simple simulation example is used initially to clearly explain the methodology. The results of identifying a model from a real crystal growth experiment show that the proposed method can produce a good representation of crystal growth.

1 Introduction

Considerable theoretical and experimental effort has been expended in an attempt to develop a better understanding of growth processes that are controlled by the energetics of the curved phase boundary. One of the most common examples of these processes is the growth of crystals, which starts from the nucleation stage and grows following specific laws. Patterns generated by growth processes can be partially represented in terms of characteristic length, such as the thickness of a branch, the distance between two branches and the curvature of the branch tips. The investigation of these characteristic

---

*Department of Automatic Control and System Engineering, University of Sheffield, UK.

†Department of Chemical and Process Engineering, University of Sheffield, UK.

lengths and the laws on which they depend for growth, using experimental, theoretical and computer simulation methods, have played an important role in understanding these important and little understood natural phenomena.

A wide range of mathematical models have now been developed to simulate the growth dynamics of crystals. The Eden model [1],[2], initially developed to investigate the growth of biological cell colonies, and the diffusion-limited aggregation (DLA) model [3], one of the most striking examples of the generation of a complex disorderly pattern by a simple model, have been widely used in biology, colloid science and materials science [4]-[7]. However, very few authors have studied the inverse problem of how to extract or identify simple mathematical descriptions directly from observed experimental growth data. A Cellular Automata model has been used to identify crystal growth based on neighbourhood detection and parameter estimation of a polynomial model in [9], where the results are encouraging. But it is not easy to link the terms of the model with the physical variables in the experiment, such as solution concentration and temperature etc. Ideally, the identified mathematical representation should be a function of the physical variables. The model obtained can then easily be used to predict the crystal pattern for a given set of particular physical variables at a particular time. In this paper, the focus is on developing an identification algorithm using a polynomial model based on the relationship between kinetics and morphology of dendritic crystals.

This approach has been shown to be correct for a few well characterized material systems, where all the thermochemical constants are accurately known, and where the basic relationship that controls the kinetics and morphology of dendritic crystals can be shown to be of the form [10]

$$VR^2 = 2\alpha cT/\delta^* L \tag{1}$$

where V is the tip speed; R is the tip radius of curvature; α is the thermal diffusivity; c and L are the specific and latent heat respectively; δ^* is the stability parameter. In practice, although some parameters in Eqn.(1) are not easy to be measured quantitatively. It should be possible to determine a relationship between tip speed and curvature assuming all the other physical variables are fixed. By repeating the experiment and identification with different physical conditions, the connection between terms and coefficients of the identified model and the physical variables can be finally linked.

The study begins in Sec.2 with a description of how to identify the underlying relation-

ship between kinetics and morphology assisted by a simple example. In Sec.3 methods to identify a model from a real crystal growth experiment using the new method is introduced. Finally, conclusions are give in Sec.4.

2   Identification based on Curvature and Growth Velocity

This section describes the procedure to identify a polynomial model based on curvature and growth velocity associated with boundary prediction based on the generated model. To assist the explanation of the methodology, a simple example will be used to illustrate the procedure. The identification method can easily be extended to other more complex cases.

2.1   Curvature Calculation

Curvature can be defined as the amount of the degree of bending of a mathematical curve, or the tendency at any point to depart from a tangent drawn to the curve at that point. Traditionally, curvature of a point on a curve can be obtained by finding a circle that "fits" the curve at that point. The reciprocal of the radius of that circle is defined as the curvature of the considered point. For example, the curvature value k of each point on a circle with radius r is $\frac{1}{r}$.

Consider a continuous system which can be expressed by $y = f(x)$. In mathematics, the curvature function of this system can be expressed as [14]

$$k(x) = \frac{f''(x)}{(1+f'(x)^2)^{3/2}} \qquad (2)$$

If the mathematical expression of the considered curve is known, it is easy to calculate the curvature at each point by Eqn.(2). However, the objective which is the focus in this paper is the boundary of a crystal, which is composed of a group of discrete pixels in a captured two-dimensional image. It is therefore not easy to find a continuous mathematical model to represent the considered boundary before the curvature calculation. Based on the properties of a crystal boundary in a digital image, such as data limitations and boundary discontinuities etc., this paper will employ a modified *three-point-method* to

3

calculate the curvature of each pixel on a boundary.

Initially, pixels on the considered boundary are sorted into an array $\{b_i = (x_i, y_i) : i = 1, 2, ..., n\}$ based on a boundary walk, which means that b_i, b_{i+1} are adjacent. The symbol n denotes the total number of pixels on the boundary, and (x_i, y_i) denotes the pixel position in the image. Because boundary of a crystal is closed, b_1, b_n are adjacent as well, which makes the array a circle chain.

Consider the pixel b_i, whose curvature, denoted by k_i, can be determined by collecting three pixels $\{b_{i-h}, b_i, b_{i+h}\}$ and then finding a circle which goes through all three pixels according to the *three-point-method*. The symbol h, which is a very important parameter, denotes the **sampling interval**. Assume that the radius of the circle is r_i, if $h \to 0$, k_i can be expressed as

$$k_i = \frac{1}{r_i} \tag{3}$$

In practice, $\frac{1}{r_i}$ is an approximate value for the curvature because the condition $h \to 0$ will never be satisfied. Theoretically, the closer h is to 0, the more accurate k_i is. Figure 1 shows an example, where different sampling intervals are used to calculate the curvature at point $(0, 1)$ on $y = cos(x)$. According to Eqn.(2), the curvature at point $(0, 1)$ is 1. Inspection of Figure 1 shows that the top-left graph, which uses the smallest h, produces the best result. However, any noise, such as a small bump, can easily and dramatically effect the result using a small h. Hence, it is very important to find an appropriate sampling interval which can not only effectively reduce noise interference, but also can generate a relatively accurate curvature.

Consider the boundary shown in Figure 2. According to the above discussion, to calculate the curvature at position A accurately, a large h should be chosen to reduce the effects of small amounts of noise , whereas to calculate the curvature at position C a small h should be chosen because of the rapidly changing curvature at that point. Hence, a variable sampling interval is introduced in this paper. Basically, this is a *coarse-to-fine* method, where the curvature at each pixel is calculated twice. Initially, the curvature of the considered pixel is calculated roughly using a fixed h. A new sampling interval, which is used in the second calculation, is re-assigned based on a nonlinear model to provide the best h for each specific curvature. Finally, the curvature is refined by using the new h in the second calculation.

Consider the example shown in Figure 2. The array of boundary pixels starts from
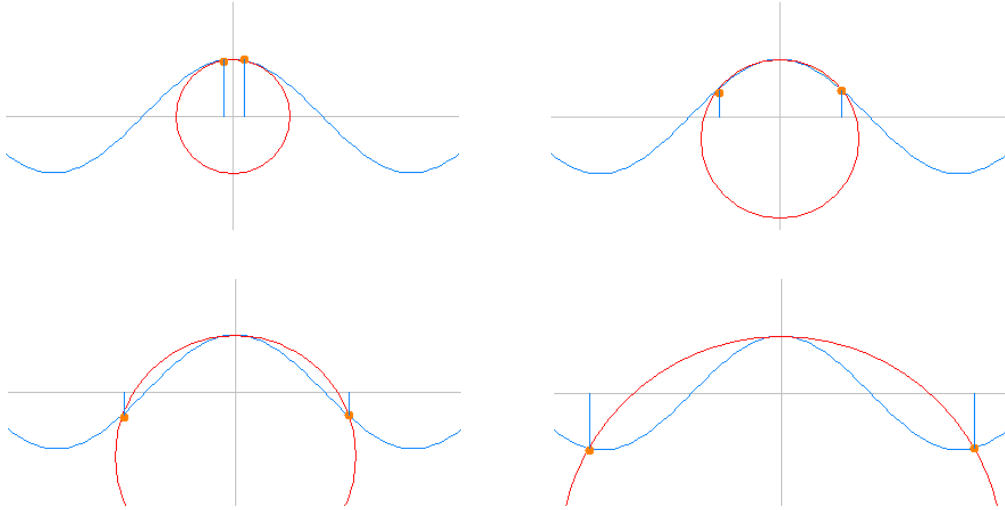
Figure 1: Curvature calculation using three-point-method with different sampling interval.
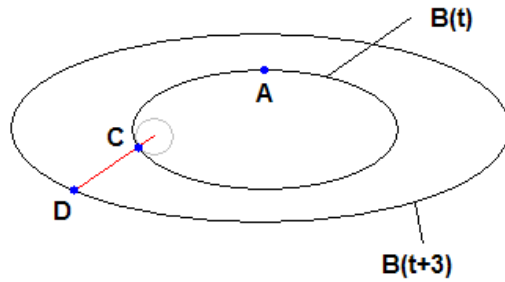

Figure 2: A simulation example for crystal boundary evolution

pixel A in a clockwise direction. Figure 4(a) shows the calculated curvature values using a fixed sampling interval ($h = 31$), which can be viewed as a coarse curvature choice, or the result from the traditional method. A simple non-linear model, which is illustrated in Figure 3(a), was used to re-assign h. A comparison of the initial h and the re-assigned h for all pixels in the array is shown in Figure 3(b). Figure 3(b) clearly demonstrates that pixels with large curvature were assigned a small h and pixels with small curvature were assigned a relatively large h. Figure 4(b) shows the calculated curvature values using the re-assigned h. Inspection of the curvature comparison when using a fixed h and a variable h, illustrated by Figure 4(c), clearly shows the variable sampling interval can produce a smoother and more accurate estimation of curvature. A two-dimensional form for Figure 4(b) is shown in Figure 4(d), where the length and direction of the arrows denote the value and direction of the curvature respectively. Note that in a
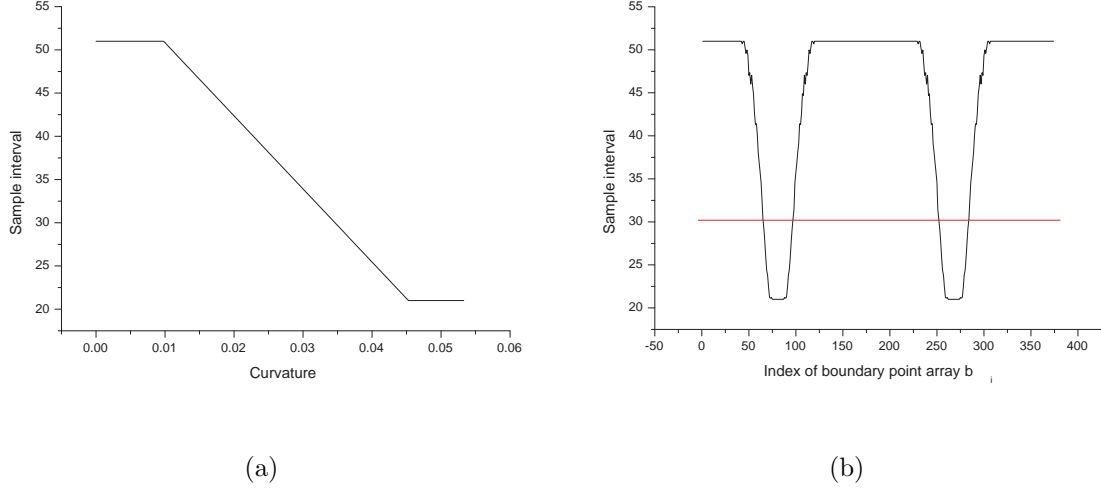
(a)   (b)

Figure 3: (a) A non-linear model to re-assign the sampling interval; (b)Sampling interval of all pixels on the boundary where the red line denotes the initial h and the black curve denotes re-assigned h.

a real crystal growth experiment, concave boundaries with large curvature are almost motionless. In the contrast, convex boundaries with the same curvature lead to grow fast. To accommodate these effects in this paper, the curvature of convex pixels on the boundary will be calculated as normal, but the curvature of concave pixels will be assigned as zero. The concepts of convex pixel and concave pixel boundaries only exist for close boundaries.
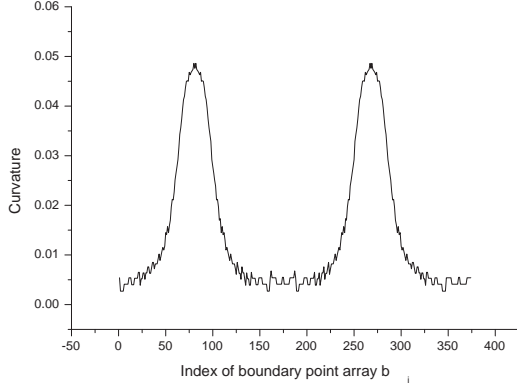
2.2   Growth Speed Calculation

In Figure 2, $B(t)$ and $B(t + 3)$ denote the boundary of a crystal at time t and $t + 3$ respectively. Consider a pixel C on boundary $B(t)$. Assume that the calculated curvature at pixel $C = (c_x, c_y)$ is k_c and the center of the fitted circle is at the position $C_R = (c_{rx}, c_{ry})$, determined by the method above. Obviously,

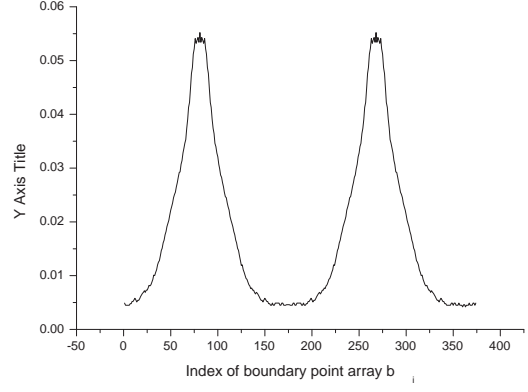$$k_c = ((c_x - c_{rx})^2 + (c_y - c_{ry})^2)^{-1/2} \qquad (4)$$

In this paper, the direction of evolution at pixel C, θ_C, is defined as the direction from C_R to C. The mathematical form of θ_C can be expressed as

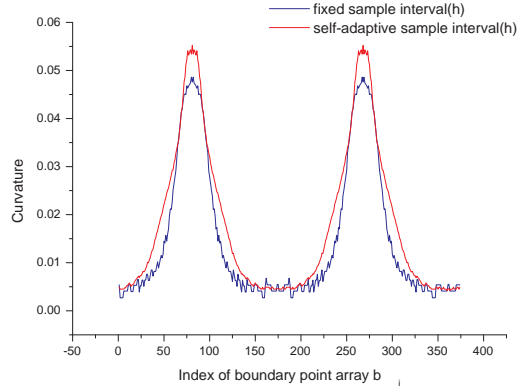$$\theta_C = arctan(\tfrac{c_y - c_{ry}}{c_x - c_{rx}}) \qquad (5)$$

As illustrated in Figure 2, a line was drawn starting from pixel C in the direction θ_C eventually crossing $B(t + 3)$ at point D. Point D can be viewed as the next position of
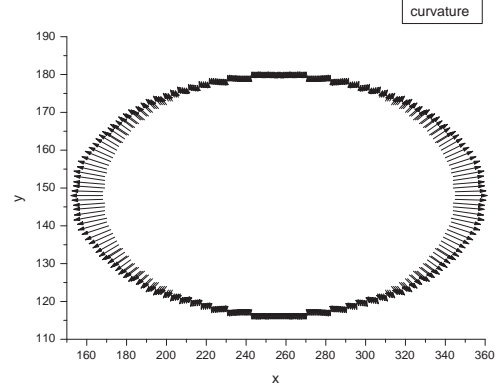
6

Figure 4: (a) Calculated curvature using a fixed sampling interval; (b) Calculated curvature using a variable sampling interval; (c) Comparison of curvatures using the fixed and variable sampling interval; (d) Curvature illustration using a variable sampling interval in two-dimension

pixel C at time $t + 3$. Therefore, the velocity of C, denoted by $\vec{v_C}$, can be described as

$$
\begin{aligned}
|\vec{v_C}| &= \frac{\sqrt{(c_x - c_{rx})^2 + (c_y - c_{ry})^2}}{4} \\
\angle \vec{v_C} &= arctg(\frac{c_y - c_{ry}}{c_x - c_{rx}})
\end{aligned}
\tag{6}
$$

The calculated velocity of the boundary is shown in Figure 5, where the left and right boundaries grow much faster than the top and bottom parts, which is consistent with the curvature illustration, shown in Figure 4.(d).
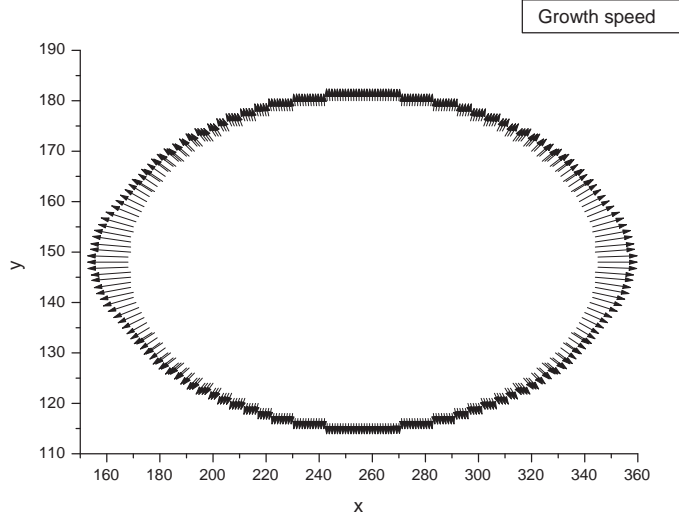
Figure 5: Calculated velocity for the example in Figure 2

2.3 Model Estimation

As shown in Eqn.(1), the rate of variation in crystal size is related to the local curvature of a branch. Inspired by the similarity between Figure 4(d) and Figure 5, the present study attempts to use a polynomial model to represent the underlying connection between curvature and growth speed. The structure of the polynomial model can be expressed as

$$v = a_0 + a_1 k + a_2 k^2 + ... + a_d k^d \tag{7}$$

where v denotes growth speed, k denotes curvature and d is the order of the polynomial model. The coefficients $\{a_0, a_1, ..., a_d\}$ can be estimated by orthogonal least squares [12] from collected training data pairs. Both second and the third order polynomial models were estimated and given in Eqn.(8) below. Figure 6, which compares the collected training data pairs with the second and third order polynomial models shows that both models fit the training data well.

$$\begin{aligned}
v &= 34.88528 - 74.4495k + 29286.5635k^2 \\
v &= 26.49301 + 1736.43603k - 53143.91017k^2 + 980621.179k^3
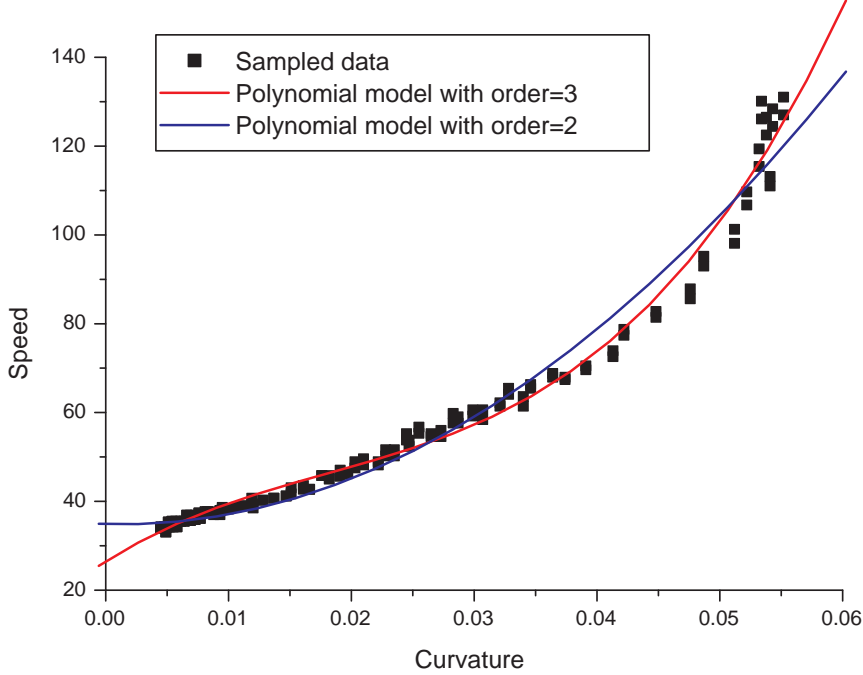\end{aligned} \tag{8}$$

Figure 6: Estimated polynomial models using orthogonal least squares

2.4 Boundary Prediction

To evaluate the goodness of the generated model, a common solution is to compare the original pattern with the prediction from the model.

Consider a pixel $E_t = (x_{E_t}, y_{E_t})$ on a boundary at time t for example, the onetime-step-ahead(OSA) prediction of E_t is only determined by the estimated speed $\vec{v_{E_t}}$, which can be obtained by Eqn.(6) and Eqn.(7) according to the curvature of E_t. Assuming the growth speed of each pixel at time t is the same as that at time $t-1$, the OSA prediction of pixel E_t at time $t+1$ can then be expressed as

$$
\begin{aligned}
x_{E_{t+1}} &= x_{E_t} + |\vec{v_{E_t}}| \times cos(\angle \vec{v_{E_t}}) \\
y_{E_{t+1}} &= y_{E_t} + |\vec{v_{E_t}}| \times sin(\angle \vec{v_{E_t}})
\end{aligned}
\tag{9}
$$

Based on Eqn.(9), the OSA prediction can be produced for every pixel on the boundary at time $t$to form a new boundary for time $t+1$. However, the new boundary will not be a closed boundary because gaps may exist between E_{t+1} and F_{t+1} if E_t and F_t are connected together. As shown in Figure **??**, the red pixels represent the predicted boundary, which is cut into lots of small sections and this is likely to bring problems at the next time

step. Hence, before producing the OSA prediction for time $t+2$ based on the predicted boundary at time $t+1$, the broken boundary must be connected together. The simplest way is to connect adjacent pixels with a smallest distance using a line. However, any slight noise can make the connected boundary zigzag. There are many methods which can be used to smooth the boundary, such as polynomial fitting, parabola fitting and B-splines. In this paper, the discrete boundary is divided into several parts and each part is interpolated by an estimated polynomial model.

To demonstrate the effectiveness of the sampling interval and the polynomial model order, several one-step-ahead predictions of A_t in Figure 2 using different h and d values are shown in Figure 7, where the red pixels denote the predicted position for the boundary at time $t+1$. The inner black part is the boundary at time t and the outer black part is the boundary at time $t+1$. The selection of sampling interval however can dramatically affect the prediction result. Too small a value for h, as shown in Figure 7(a), or too large a value of h, as shown in Figure 7(d), will produce poor predictions. Figure 7(c), the prediction produced by a variable h, obviously demonstrates better performance than those of fixed h. Therefore, the proposed method to choose a self-adaptive sampling interval is very important for achieving a good representation of boundary growth. Inspection of Figure 7(c) and 7(d) shows the polynomial model order has much less influence on the prediction compared with the sampling interval.
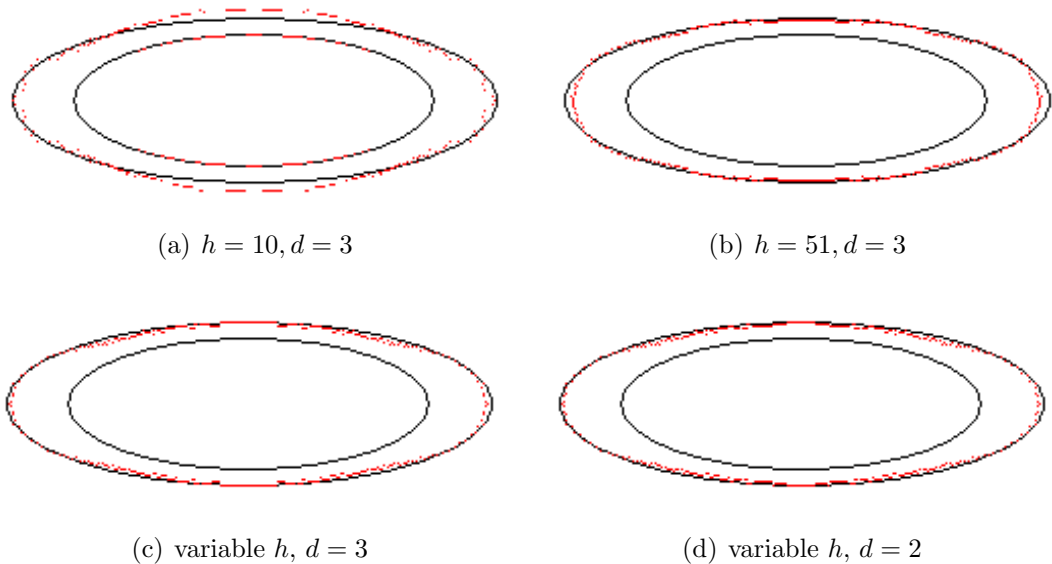

(a) $h = 10, d = 3$

(b) $h = 51, d = 3$

(c) variable h, $d = 3$

(d) variable h, $d = 2$

Figure 7: OSA predictions using different sampling intervals and polynomial orders for the example.

3   Example

To evaluate the efficiency of the proposed method when applied to real systems, a NH_4Br crystal growth experiment was conducted. Crystal size changes in the spatio and temporal dimensions are shown in Figure 8, which includes three original image snapshots and the preprocessed images respectively extracted from a group of experiment data. Details regarding the experimental setup and preprocessing of the captured images can be found in [11]. The purpose of this study is to generate a mathematical model which can quantitatively define the relationship between the curvature of a boundary and the speed of growth. OSA predictions can then be produced and compared with the original images, to validate the model. To illustrate the growth of such a slow system, the
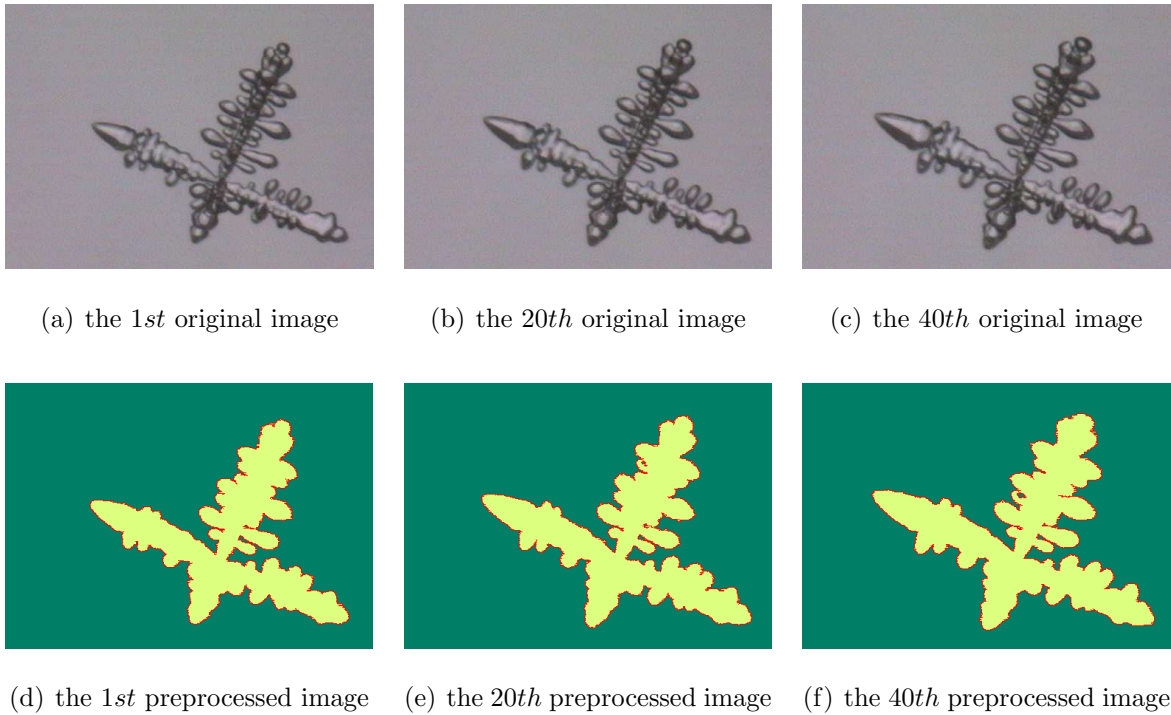

(a) the $1st$ original image   (b) the $20th$ original image   (c) the $40th$ original image

(d) the $1st$ preprocessed image   (e) the $20th$ preprocessed image   (f) the $40th$ preprocessed image

Figure 8: Three snapshots and preprocessed images

overlay of the 1st and the 22nd original sampled frame is shown in Figure 9(a), where the black part denotes the 1st frame and the red part denotes the 22nd frame. Ideally, the proposed method should generate a global mathematical model by sampling all the data. However, there are always some inevitable factors that effect different regions so that locally the growth patterns may be different. Noise, for example, caused by image aberrance, which always happens in a normal lens of image acquisition equipment, will

have an influence on the four corners of the image, but has much less influence on the central part. This could slightly change the rule of the regions near the boundary. Hence, it is reasonable to focus on a specific branch of the crystal instead of the whole image during identification. A large image can be viewed as a composition of several regions, each of which can be identified separately. The whole pattern can then be reconstructed by combining the prediction of each part.

Consider therefore just the bottom-right branch in Figure 9(a), shown in Figure
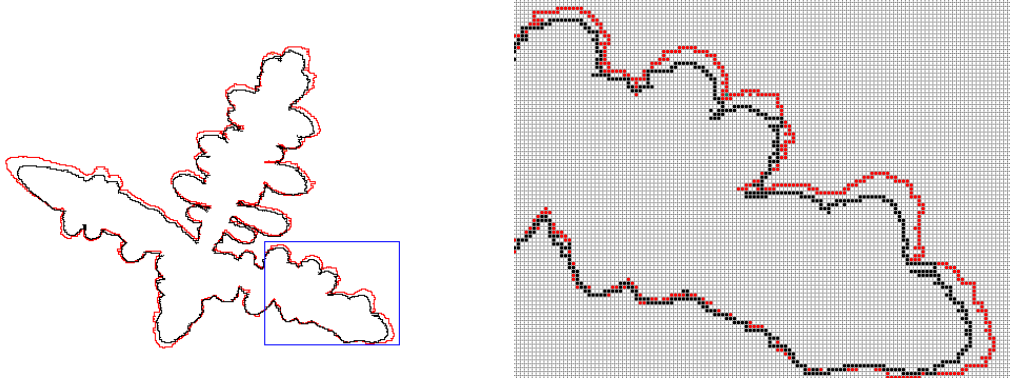

Figure 9: (a) Overlay of the 1st and 22nd whole sampled frame; (b) Overlay of the 1st and 22nd of the focused region.

9(b), which clearly demonstrates the characteristic of crystal growth in this experiment. Bumps with large curvature grow faster than flat or concave boundaries, which suggested the use of the method proposed in this paper to identify the underlying laws. First 22 frames were sampled and the calculated curvature of the 22nd frame using a variable sampling interval is shown in Figure 10(a). Figure 10(b) shows the growth velocity based on the growth direction derived from the previous step. A polynomial model was then identified by fitting the collected data pairs of curvature and growth speed, which can be expressed as:

$$v = 1.2105 + 129.34k - 954.85k^2 \tag{10}$$

To validate if this simple model can represent such a relatively complex system, the 42th frame was predicted based on the OSA. Figure 11(a) shows an overlay of the predicted 42th frame (red boundary) and the original 42th frame (black boundary), and shows that the predicted boundary is very close to the original one. Although the prediction is not exactly the same as the original this is to be expected because of the presence of noise
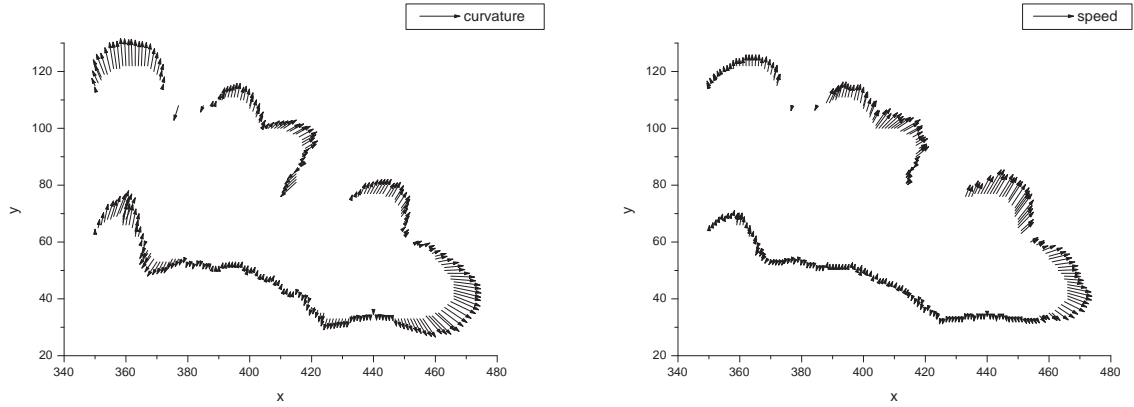
Figure 10: (a) Calculated curvature for the focused region ; (b) Detected speed for the focused region.

introduced by the equipment and image preprocessing. However, the prediction does capture the main growth characteristics in this real example, which indicates that the identified model is a good representation of the considered region.

The identified model from the right-bottom branch was also used to predict growth over the whole crystal. The predicted 42nd frame, the original data for the whole crystal are shown in Figure 11(b). The results clearly demonstrate that the prediction of the left branch is much worse than for other parts, which indicates that the rule for the left branch may be different. Further investigations will focus on how to identify a single crystal growth model composed of regions with different rules.
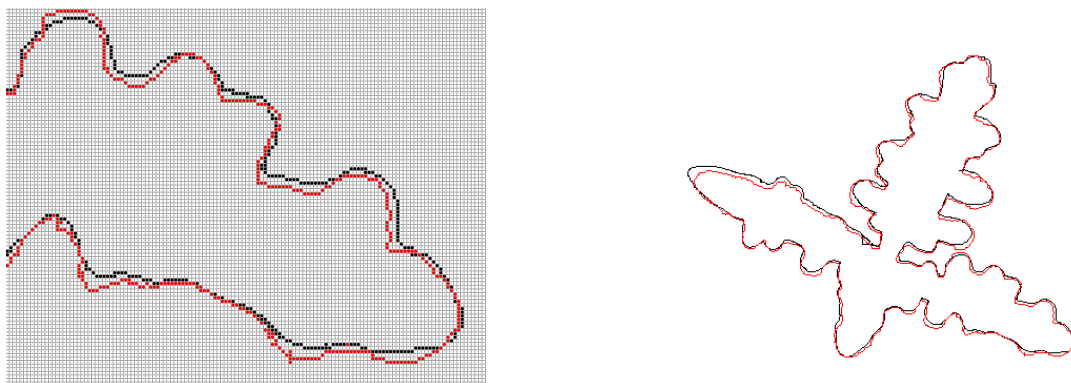

Figure 11: (a) Overlay of the predicted 42th frame and the original 42th frame of the focused region; (b) Overlay of the predicted 42th frame and the original 42th frame of the whole crystal.

4 Conclusions

A new identification method for crystal growth based on a tip curvature-velocity relationship has been introduced. Before modelling, it is very important to accurately calculate curvature for each pixel along the considered boundary. The well known three-point method was modified in this paper by introducing a variable sampling interval to calculate curvature. The results shown in Figure 1 clearly indicate this method has a better performance than for boundaries whose the curvature is considerably changed in the spatio dimension. A multi-order polynomial was then identified to represent the relationship between curvature and velocity. The model is consistent with the model shown in Eqn.(1), which provides the possibility of linking the identified model with physical variables that affect the morphology of the crystal.

A real NH_4Br crystal growth experiment was conducted and the acquired data were analysed using the proposed method. Although it is impossible to predict crystal growth exactly, the results shown in Figure 10 are very encouraging. The prediction from a relatively simple model captures the characteristics of boundaries with large curvature growths.

Identification of real systems is often very difficult because of the many factors involved. In this paper, one small branch was sampled and modelled initially. When the generated model was used for other branches, the predictions were not all perfect. This may due to the rotation of the crystal, aberrations in the lens or other equipment factors. Many more experiments need to be conducted and the link between the identified model and the environmental and control parameters needs to be investigated in further studies.

Acknowledgment

References

[1] Murray Eden, "A two-dimensional growth process," *4th. Berkeley symposium on mathematics statistics and probability*, vol.4, pp.223-239, 1956.

[2] Murry Eden, "A probabilistics model for morphogenisis," *Symposium on imformation theory in bilogy*, vol.29-31, pp.359-370, 1956.

[3] T.A. Witten and L.M. Sander, "Diffusion-limited Aggregation, a Kinetic Critical Phenomenon", *Physical REview Letters*, vol.47, pp.1400-1403, 1981.

[4] T.Williams and R.Rjerknes, "Stochastic model for abnormal clone spread through epithelial based layer," *Nature*, vol.236, pp.19-21, 1972.

[5] D.Mollison, "Conjecture on the spread of infection in two dimensions disproved," *Nature*, vol.240, pp.467-768, 1972.

[6] P.Meakin, "Cluster-growth processes on a two-diemensional lattice," *Physical Review*, vo.B28, pp.6718-6732, 1983.

[7] M.J.Vold, "Computer simulation of floc formation in a colloidal suspension," *Journal of colloid science*, vol.18, pp.684-695, 1963

[8] Paul Meakin, *Fractals, scaling and growth far from equilibrium*, Cambridge university Press, 1998.

[9] Y.Zhao and S.A.Bilings, "Identification of Crystal Growth using Cellular Automata Models", Research Report No.593 of AC&SE, University of Sheffield, 2007.

[10] M.E.Glicksman and S.C. Huang, "Convective Heat Transfer During Dendritic Growth", Convective Transport and Instability Phenomena, ed. Zierep and Ortel, Karlsruhe, (1982), 557.

[11] Y.Zhao and S.A.Billings, "Identification of the Belousov-Zhabotinskii Reaction using Cellular Automata Models", *International Journal of Bifucation and Chaos*, vol.17, No.5, pp.1687-1701, 2007.

[12] M.Korenberg, S.A.Billings, "Orthogonal parameter estimation algorithm for nonlinear stochastic systems," *International journal of control*, vol.48, no.1, pp.193-210, 1988.

[13] M.E.Glicksman, "Effects of crystal-melt interfacial energy anisotropy on dedritic morphology and growth kinetics," *Journal of Crystal Grwoth*, vol.98, pp.277-284, 1989.

[14] R.C.Yates, "Curvature," A Handbook on Curves and Their Properties. Ann Arbor, MI: J. W. Edwards, pp.60-64, 1952.